

# Point2Act: Efficient 3D Distillation of Multimodal LLMs for Zero-Shot Context-Aware Grasping

Sang Min Kim<sup>1</sup> Hyeongjun Heo<sup>1</sup> Junho Kim<sup>1</sup> Yonghyeon Lee<sup>2</sup> Young Min Kim<sup>1</sup>  
<sup>1</sup>Seoul National University, <sup>2</sup>Massachusetts Institute of Technology  
 {tkdals9082, heo0224, 82magnolia}@snu.ac.kr, yhl@mit.edu, youngmin.kim@snu.ac.kr



Figure 1: We present Point2Act, which grounds natural language into localized 3D fields by distilling Multimodal LLMs, bridging semantic understanding and physical interaction in robotic tasks.

**Abstract:** We propose **Point2Act**, which directly retrieves the 3D action point relevant for a contextually described task, leveraging Multimodal Large Language Models (MLLMs). Foundation models opened the possibility for generalist robots that can perform a zero-shot task following natural language descriptions within an unseen environment. While the semantics obtained from large-scale image and language datasets provide contextual understanding in 2D images, the rich yet nuanced features deduce blurry 2D regions and struggle to find precise 3D locations for actions. Our proposed *3D relevancy fields* bypass the high-dimensional features and instead efficiently imbue lightweight 2D point-level guidance tailored to the task-specific action. The multi-view aggregation effectively compensates for misalignments due to geometric ambiguities, such as occlusion, or semantic uncertainties inherent in the language descriptions. The output region is highly localized, reasoning fine-grained 3D spatial context that can directly transfer to an explicit position for physical action at the on-the-fly reconstruction of the scene. Our full-stack pipeline, which includes capturing, MLLM querying, 3D reconstruction, and grasp pose extraction, generates spatially grounded responses in under 20 seconds, facilitating practical manipulation tasks. Project page: <https://sangminkim-99.github.io/point2act/>

## 1 Introduction

Robotic systems are increasingly expected to interpret and act on natural, context-rich human language. Recently, the integration of vision language models (VLMs) – including CLIP [1] and Multimodal Large Language Models (MLLMs) – with 3D representations has opened new possibilities for partially addressing this problem [2, 3, 4, 5, 6, 7, 8]. Despite their promise, leveraging VLMs exhibits key challenges in *efficiency* while concurrently achieving *high spatial precision*. The high

dimensionality of vision-language features (e.g.,  $>512$ ) renders the construction of 3D feature fields computationally expensive and memory-intensive, typically requiring 1–2 minutes per scene. In addition, they often struggle with tasks that require precise 3D localization of spatially specific points (e.g., picking up a small tool from a cluttered tray), as similarity maps tend to produce diffuse activations in 2D images, which can vary depending on the viewpoint. Most importantly, these models frequently fail to interpret compositional descriptions and capture subtle contextual nuances [5, 6]. For instance, instructions such as “the cap of black marker outside the paper” involve hierarchical spatial and semantic reasoning that remains challenging for current systems.

We propose **Point2Act**, which scrutinizes the task-specific action point in 3D, conditioned on language instructions that encompass zero-shot tasks across a broad spectrum. Point2Act suggests that our ultimate objective – shared by many existing approaches – is to accurately identify a semantically relevant 3D point for manipulation. In this regard, the dense 3D field with high-dimensional features is redundant and can even complicate fine-grained spatial grounding. Instead, we prompt an MLLM to directly produce 2D-relevant points from multi-view images and efficiently aggregate them to infer 3D-relevant points. The resulting *3D relevancy field* encodes single-channel relevancy information with precise spatial localization, addressing the key limitations of prior work; see Figure 5. Equipped with fine-grained localization of enhanced contextual reasoning, our method demonstrates the compositional capability to concurrently derive and respect complex semantic constraints, beyond what previous methods could achieve (see Figure 1).

To enable real-world deployment, we develop an efficient full-stack pipeline that integrates multi-view image capture, MLLM querying, 3D scene reconstruction, and grasp pose extraction. While the point-based interface is token-efficient, querying the MLLM for each view takes approximately 1–2 seconds. We address this latency by carefully pipelining the process, enabling generation of actionable 3D relevancy fields in about 20 seconds – significantly faster than comparable methods.

Our contributions are:

- We propose Point2Act, which distills multi-view MLLM point outputs into 3D relevancy fields to achieve high-level spatial grounding robust to occlusions and view changes.
- We enable zero-shot context-aware robotic tasks by supporting part-aware, spatial, and even abstract language queries – such as “the handle of the red mug,” “the center of the monitor stand,” or “a dangerous part that can hurt a human hand.”
- We build a practical, efficient system deployable in real-world settings within  $\sim 20$ s.

## 2 Related Work

### 2.1 3D Feature Fields for Robotic Manipulation

Recent advances in 3D scene representations, such as Neural Radiance Fields (NeRF) [9] and Gaussian Splatting [10], have enabled the reconstruction of high-quality 3D scenes from multi-view images. Beyond raw RGB values, recent approaches leverage foundation models to lift image content into rich feature fields that encode diverse types of information—such as language [2, 3, 4, 11], semantics [12, 13, 14], and affordances [8]—depending on downstream tasks. These feature fields have been successfully utilized for a wide range of robotic tasks, including navigation [15, 16, 17], grasping [18, 19, 20, 21], and object rearrangement [7, 22]. Our work is inspired by LERF-TOGO [6], which builds on LERF [3] to distill high-dimensional language-embedded features into a 3D field for zero-shot robot manipulation. Unlike LERF and its variants, our method prompts MLLM to directly predict 2D points from language queries, which are then distilled into 3D relevancy fields. Such a design choice enables efficient and spatially grounded grasping.

### 2.2 Large Language Models for Robotics

Recent advances in LLMs have driven a surge of interest in applying their reasoning capabilities to robotics. A prominent line of work leverages LLMs as general-purpose planners by prompt-

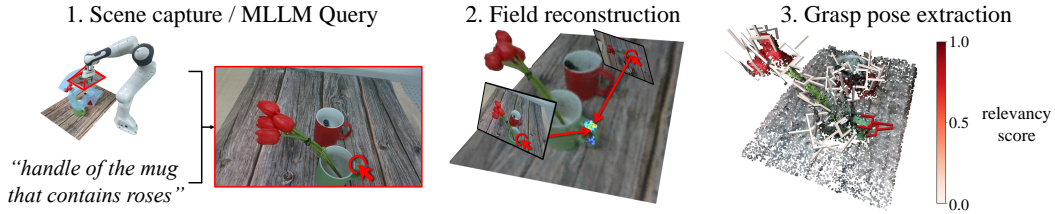


Figure 2: Overview of the **Point2Act** pipeline. We first capture posed images and query the MLLM [39] with a prompt to predict 2D point annotations on the images. The multiview predictions are distilled into a 3D relevancy field. AnyGrasp [40] proposes grasp candidates, and the most relevant grasp is selected based on the field. Grasp poses are subsampled for visualization.

ing them to generate executable robot code or skill sequences from natural language instructions, grounded through pretrained policies or APIs [23, 24, 25, 26]. While promising, these approaches often depend on fragile code-generation pipelines, handcrafted prompts, API-specific infrastructure, and careful output parsing. Another stream of research focuses on training Vision-Language-Action (VLA) models that unify perception, language understanding, and control within a single architecture, incorporating LLMs or MLLMs as integral components [27, 28, 29, 30, 31]. These models are trained on large-scale robot demonstration datasets and have shown impressive generalization ability across diverse tasks. However, they tend to struggle in out-of-distribution scenarios and typically require additional demonstrations or fine-tuning to adapt to novel environments. Our method bypasses both code synthesis and end-to-end policy learning by distilling token-efficient 2D predictions from a pretrained MLLM into compact 3D relevancy fields.

### 2.3 Context-Aware Grasping

Beyond simply achieving a stable grasp, the appropriate grasping location may vary depending on the subsequent task, necessitating task-oriented grasping [32, 6, 33, 34, 35]. In some cases, it is essential to consider not only the task but also the broader context surrounding the object and the scene. For instance, Liu et al. [36] incorporates both object-level factors and task-level requirements for contextual grasp planning. Besides, Hoang et al. [37] performs grasping in cluttered scenes by leveraging the surrounding scene geometry as contextual information, rather than focusing solely on a single object. A recent study by Jin et al. [38] tackles a task closely related to ours. While their approach relies on 2D representations and task-specific fine-tuning, our method constructs spatially grounded 3D relevancy fields by distilling knowledge from a pretrained MLLM across multi-view observations. This enables more robust and generalizable grasping. Further, our framework is applicable to additional manipulation tasks beyond grasping, highlighting its broader utility.

## 3 Method

Point2Act provides highly localized 3D positions, jointly considering both the spatial context of the scene and the additional semantics required by human instruction. The resulting representation can subsequently solve the problem referred to as *context-aware grasping*, where the goal is to predict the appropriate 6-DOF grasp pose in the scene to fulfill the contextual description. To solve this problem, Point2Act inquires MLLMs to produce point-wise outputs that not only locate the target object but also consider scene-level context and part-level analysis, reasoning compounded conditions that are not explicitly stated within the instruction. We then aggregate the estimated points from multiple images into a localized 3D region. While inference with MLLMs may be computationally intensive, we formulate a practical pipeline that efficiently allocates tasks across different temporal stages, minimizing waiting times within a reasonable range. The 3D representation with physical grounding is lightweight, and we geometrically predict a firm 6-DoF grasp (or any other necessary actions for the task) around the found position, independent of complex reasoning processes.

We first describe the *3D relevance fields*, which reconstruct the 3D scene and the action point in the form of a neural field representation (Section 3.1). Using simplified spatial grounding, we generate a sequence of physical actions of a robot to fulfill the given task (Section 3.2). Finally, we describe an efficient pipeline for real-world deployment with on-the-fly 3D reconstruction and multiple queries to the MLLMs (Section 3.3). The overview of the Point2Act pipeline is shown in Figure 2.

### 3.1 Relevancy Field Distillation from MLLM

Given a natural language instruction, the robot captures scene images from which we build a 3D relevancy field. The field encodes both scene geometry and a language-grounded relevancy of each 3D position  $\mathbf{x} \in \mathbb{R}^3$ . Specifically, the density  $\sigma \in \mathbb{R}$  indicates the soft occupancy of surface geometry as neural radiance fields (NeRFs) [9]. We additionally assign a scalar value  $s \in [0, 1]$  of relevancy, which aggregates MLLM outputs between the position  $\mathbf{x}$  and the language instruction.

The training process extends NeRFs with an additional neural network for the relevancy score. NeRFs map a 3D position  $\mathbf{x} \in \mathbb{R}^3$  and viewing direction  $\mathbf{d} \in \mathbb{S}^2$  to color and density:

$$(\mathbf{c}, \sigma) = \text{MLP}_{\text{geo}}(\mathbf{x}, \mathbf{d}), \quad (1)$$

where  $\mathbf{c}$  is RGB color and  $\sigma$  is volume density. The rendered color along a ray  $\mathbf{r}(t) = \mathbf{o} + t\mathbf{d}$  from origin  $\mathbf{o}$  with direction  $\mathbf{d}$  is computed as

$$\hat{\mathbf{C}}(\mathbf{r}) = \int_{t_n}^{t_f} T(t)\sigma(\mathbf{r}(t))\mathbf{c}(\mathbf{r}(t), \mathbf{d})dt, \quad (2)$$

where  $T(t) = \exp\left(-\int_{t_n}^t \sigma(\mathbf{r}(x))dx\right)$  is the accumulated transmittance. The geometry branch  $\text{MLP}_{\text{geo}}$ , which follows the conventional formulation of NeRFs, is trained by minimizing the squared error between the rendered color  $\hat{\mathbf{C}}(\mathbf{r})$  and ground-truth color  $\mathbf{C}_{\text{gt}}(\mathbf{r})$ , i.e.,  $\mathcal{L}_{\text{rgb}} = \sum_{\mathbf{r} \in \mathcal{R}} |\hat{\mathbf{C}}(\mathbf{r}) - \mathbf{C}_{\text{gt}}(\mathbf{r})|^2$ , where  $\mathcal{R}$  denotes the set of camera rays sampled across all views during training.

The relevancy is modeled with a separate, lightweight MLP that maps 3D points to scalars:

$$s = \text{MLP}_{\text{rel}}(\mathbf{x}), \quad (3)$$

with  $s \in [0, 1]$  denoting relevancy score of the 3D location  $\mathbf{x}$  tailored to the task. After the robot captures images from multiple viewpoints, each image is immediately passed to an MLLM along with the language instruction. We use Molmo [39] to obtain a simple 2D point on an image after disentangling the nuances and complex task reasoning in the instruction given visual observations. While semantic understanding from feature fields may change depending on viewpoints, the point representation unambiguously suggests the most relevant points. To allow and embrace uncertainties and misalignment in predictions, the point predictions are converted into a soft relevancy mask  $M_{\text{gt}}$  via a 2D Gaussian blur [41], producing a continuous scalar distribution. Similarly to the geometric branch, the relevancy branch  $\text{MLP}_{\text{rel}}$  is supervised using the difference between the rendered relevancy  $\hat{M}(\mathbf{r})$  and the ground-truth mask from 2D prediction  $M_{\text{gt}}(\mathbf{r})$ , defined as  $\mathcal{L}_{\text{rel}} = \sum_{\mathbf{r} \in \mathcal{R}} (\hat{M}(\mathbf{r}) - M_{\text{gt}}(\mathbf{r}))^2$ . We defer the training details to the Appendix.

As shown in Figure 5, the resulting relevancy fields suggest the Point2Act, as a fine-grained 3D region for the task action. As the multiview supervision aggregates information across views respecting the 3D scene geometry, we can effectively mitigate occlusion, misprediction, and view dependency, yielding a highly localized and view-invariant 3D guidance (Figure 6).

### 3.2 Grasping with Relevancy Fields

After learning the 3D field, we extract an appropriate sequence of action poses corresponding to the instruction. We are no longer bound to complex contextual reasoning and simply follow the low-level geometric guidance. As a widely used task, we can extract an appropriate 6-DoF grasp pose at the proposed location using an existing module with point cloud data [40]. We first convert the learned field into an RGB point cloud scene by rendering RGB, depth, and relevancy scores from

multiple viewpoints and unprojecting them into 3D space using the depth maps. We then provide the point cloud as input to AnyGrasp [40] and generate a set of grasp pose candidates.

To select the grasp pose most relevant to the instruction, we perform filtering based on the predicted relevancy field. For each grasp candidate, we extract its contact center and retrieve the  $k$  nearest neighbor points in the scene ( $k = 30$ ). Among all candidate poses, we select the one whose associated neighborhood contains the point with the highest relevancy score. This process ensures that the final grasp pose is both physically feasible and semantically aligned with the given instruction.

### 3.3 Efficient System Design

To enable real-world deployment, we optimize the full sequence – from scanning to grasp extraction – for low latency through pipelined execution. An overview of our system pipeline is shown in Figure 3. A wrist-mounted camera captures multiview images, which are sent immediately to an MLLM along with instructions to predict language-grounded points. We concurrently initialize the system and pre-load the NeRF and AnyGrasp [40] on the GPU to avoid model loading delays. Once the scanning is complete, we train the 3D field for 300 iterations: the first 200 optimize only appearance and geometry, then jointly with relevancy. At iteration 200, we extract an RGB point cloud and forward it to the grasping module while relevancy training continues, avoiding additional grasp inference time. Since our relevancy supervision consists of simple scalar values, the relevancy field converges rapidly, typically within 100 iterations, allowing for efficient optimization (see Figure 4(a)). Additionally, we reduce input image resolution during field construction to further accelerate training (see Appendix for ablation results). With these design choices, the entire pipeline completes in approximately 16.5 seconds, demonstrating the practicality of Point2Act in real-world scenarios.

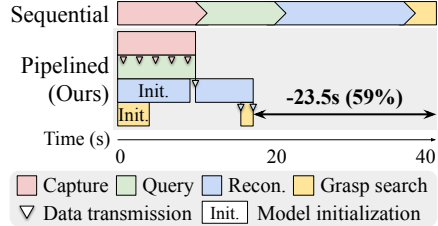


Figure 3: System diagram of Point2Act.

## 4 Experiments

We demonstrate the performance of Point2Act on a wide range of real-world examples for zero-shot context-aware grasping. We first evaluate the accuracy and efficacy of our relevancy fields (Section 4.1) and then discuss the resulting zero-shot grasping performance (Section 4.2). We then illustrate further example scenarios that require combining several contextual reasoning (Section 4.3).

### 4.1 Context-Aware 3D Localization

In this section, we analyze (1) the advantages of using lightweight MLLM-predicted 2D points as an intermediate representation and (2) the effectiveness of distilling them into a 3D field.

**Advantages of Using MLLM Points for 3D Distillation.** In this experiment, we show the effectiveness of using points from MLLMs as the distillation target for 3D localization. Specifically, we compare our method with two widely used alternatives: the multi-scale pyramid CLIP features in LERF [3] and the last layer value embeddings of MaskCLIP [42] in F3RM [5].

We evaluate 3D localization accuracy across 8 real-world tabletop scenes and 90 language prompts using two metrics. After training, each method extracts the scene point cloud and selects the most relevant 3D point based on its scoring strategy (see Appendix for details on ground truth generation and baseline scoring). *Projection accuracy* checks whether the most relevant point, when projected onto multiple camera views, falls inside the ground truth object’s mask. *Distance error* measures the distance between the most relevant point and the ground truth point cloud in 3D space.

As shown in Figure 4(a), our method quickly outperforms baselines, achieving higher accuracy and lower distance error with just **50** training iterations. This shows the strength of using sparse, highly localized MLLM point outputs, enabling fast and precise 3D grounding with minimal training.

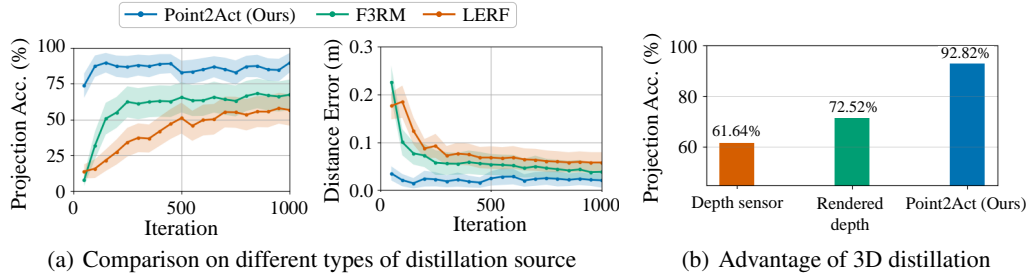


Figure 4: Quantitative results for 3D localization. (a) Localization accuracy across different language grounding methods. (b) Effectiveness of our multi-view 3D distillation. Point2Act demonstrates fast convergence and consistently outperforms all baselines.

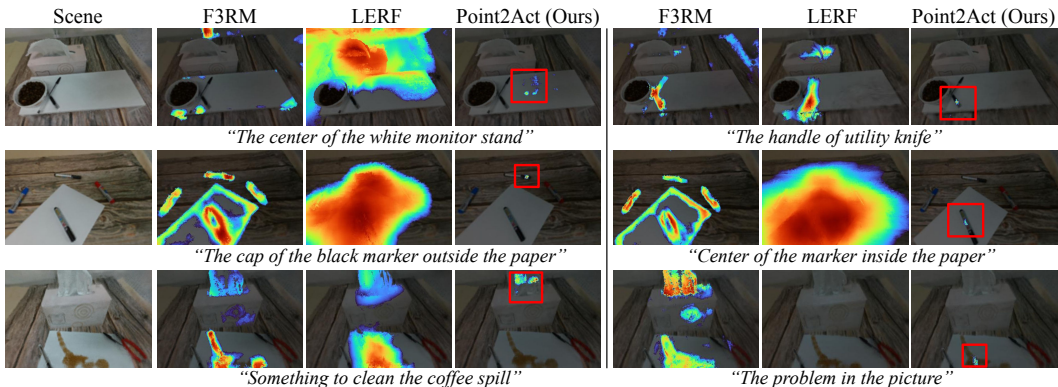


Figure 5: Comparison of language grounding methods. The first column shows the RGB render, and the others show high-relevancy scores (red: high, blue: low), overlaid on the RGB image. Prompts are shown below. Our Point2Act finds more accurate regions, highlighted with red boxes.

Figure 5 shows relevancy maps from different language grounding methods. While prior approaches produce diffuse or imprecise localization, our Point2Act produces sharp and reliable predictions. It captures spatial cues (e.g., the center of the monitor stand), relational descriptions (e.g., the cap of a marker outside the paper), and subtle user intent (e.g., selecting the tissue over the coffee spill).

**Effectiveness of Multi-view 3D Distillation.** To isolate the benefit of 3D distillation, we conduct a controlled comparison in a cluttered scene with frequent occlusions. We evaluate variants that unproject 2D point predictions into 3D using two different depth sources: (1) depth maps from a depth camera, and (2) NeRF-rendered depths after training on RGB images. While both baselines have access to 3D geometry, they rely on single-view predictions and lack true multi-view consistency.

In Figure 4(b), our Point2Act achieves the highest projection accuracy. This demonstrates the robustness of our approach to occlusion and viewpoint variation, even in complex real-world scenes (see Figure 6(a)). The rendered depth outperforms the measured depth, as depth cameras often fail to capture edge regions in the near range, resulting in missing values (see Figure 6(b)).

## 4.2 Context-Aware Zero-Shot Robotic Grasping

Leveraging strong localization capabilities, Point2Act generates plausible grasp poses in a zero-shot manner, without task-specific training. We compare Point2Act with several baselines: F3RM, LERF-TOGO, and MLLM 2D points with depth unprojection. F3RM is one of the pioneering works that distills the features of 2D foundation models (CLIP) into 3D feature fields for few-shot grasping. LERF-TOGO enhances context-level reasoning by parsing complex queries into “(object; part)” pairs using an LLM. However, both CLIP-based baselines are limited by the

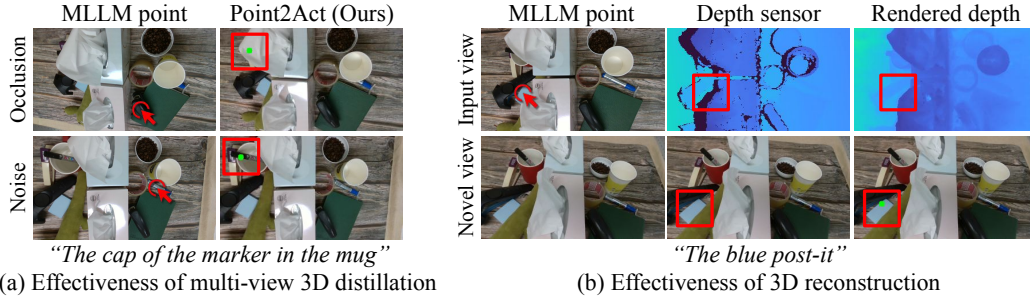


Figure 6: Effectiveness of our multi-view 3D distillation. (a) Point2Act robustly localizes relevant 3D points under occlusions and noisy MLLM outputs by aggregating multi-view cues. (b) The rendered depth fills holes near object edges, enabling correct unprojection (highlighted in red boxes).

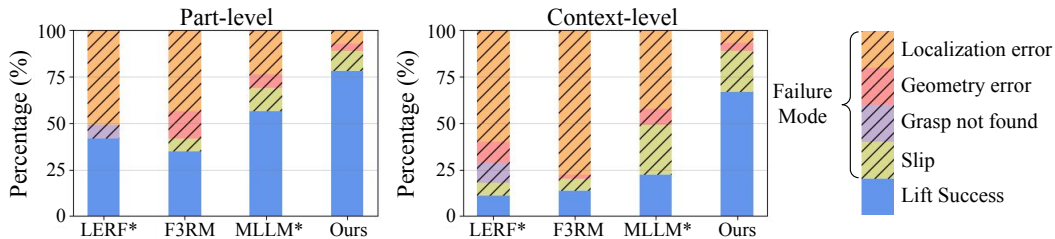


Figure 7: Grasping performance overview. Shaded areas indicate failure modes. Grasping performance evaluation is evaluated for part-level prompts (left) and context-level prompts (right). LERF\* refers to LERF-TOGO [6] and MLLM\* refers to MLLM 2D points with depth unprojection.

bag-of-words nature of CLIP features and lack fine-grained spatial and contextual understanding. MLLM with depth provides a solid baseline by leveraging MLLMs but is limited to a single view, making it vulnerable to occlusions and unable to capture essential side-view information.

We evaluate performance on four real-world tabletop scenes and 20 language prompts, with five trials per prompt. We categorize the prompts into two groups:

(1) **Part-level prompts:** These require grasping a specific part of an object (e.g., “handle of the mug”). For LERF-TOGO, we follow the original format with “object;part” pairs. For other methods, we unify the prompt format to a natural language expression such as “part of object”.

(2) **Context-level prompts:** These require interpreting the broader context of the scene or prompt. For LERF-TOGO, we process the prompt as “object;part” using ChatGPT (details are in the Appendix). These prompts typically involve either:

- **Scene context**, which involves spatial or visual reasoning, such as “the object that red scissors are pointing at” or “the item on top of the mug”.
- **Language / common-sense context**, which requires reasoning beyond the visual input, such as “something to clean the spilled coffee” (→ tissue). These prompts rely on implicit knowledge and contextual understanding rather than direct object references.

Figure 7 summarizes the grasping performance. Point2Act consistently outperforms baselines, especially in nuanced scenarios requiring spatial and language understanding. We categorize failure cases into four types. Recognition errors include localization issues and geometry errors, the latter often caused by floater artifacts on specular objects like plastic or scissors. Grasp-not-found errors are observed only in LERF-TOGO, due to its high score threshold (0.6) filtering out valid grasps. Other methods, including ours, do not apply such filtering, typically allowing at least one grasp on the target. However, some grasps fail on challenging objects such as scissor handles or kettle spouts.

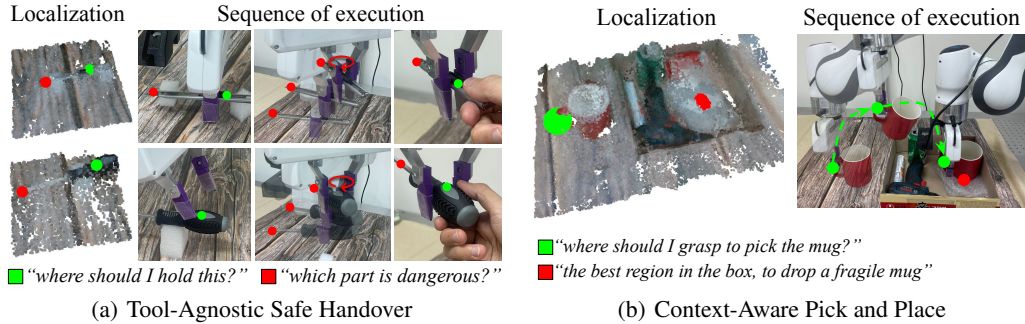


Figure 8: Qualitative results demonstrating our system’s ability to perform (a) tool-agnostic safe handover and (b) context-aware pick-and-place. In (a), green indicates the graspable region, while red marks the dangerous part that should be oriented away from the human. In (b), the system identifies both the appropriate grasp region and a safe placement area based on the scene context.

### 4.3 Downstream Applications

We explore the downstream applications of Point2Act by extending the relevancy field to two channels, enabling it to handle multiple prompts simultaneously. Since the MLLM processing time roughly doubles with two queries, we capture 16 images to ensure enough time for MLLM querying, while also enhancing the quality of the 3D reconstruction.

**Tool-Agnostic Safe Handover** In human-robot handover scenarios, the robot must orient tools to keep hazardous parts away from the human. While prior methods rely on object-specific training to detect graspable or dangerous regions [43, 44, 45], Point2Act generalizes to novel tools without additional learning. Figure 8(a) shows qualitative results using two natural language instructions: “Where should I hold this?” and “Which part is dangerous?” The robot identifies both safe grasping regions and hazardous parts, then adjusts the end-effector orientation to ensure the dangerous part faces away from the human. By distilling general knowledge from the MLLM into 3D, Point2Act works across different tools, such as a utility knife (top row) and a screwdriver (bottom row), without any tool-specific tuning. See the Appendix for further details.

**Context-Aware Pick and Place** Point2Act can identify both the graspable region and a safe placement area based on the scene context. In Figure 8(b), we show an example of context-aware pick and place. When handling fragile objects like a glass or mug, finding a safe placement area is crucial. We query two prompts: one for grasping (“where should I grasp to pick up the mug”) and another for placement (“the best region in the box to drop a fragile mug”). Point2Act successfully identifies the mug’s handle for grasping and points to the safest placement area in the box, a cushioned surface made of bubble wrap. See the Appendix for further details.

## 5 Conclusion

We present Point2Act, a practical and efficient system that combines Multimodal Large Language Models (MLLMs) with 3D field representations to address the problem of zero-shot, context-aware grasping. By using point responses as communication media with MLLMs, we distill them into a highly localized and view-independent 3D relevancy field. This sparse point signal is remarkably easy to learn, significantly reducing the number of iterations required for 3D field reconstruction. We demonstrate that the resulting 3D relevancy field enables precise spatial localization, providing a reliable guidance signal for zero-shot grasping. With our pipelined system design, the full pipeline runs in under 20 seconds, highlighting the practicality of our approach. Finally, we show that Point2Act can be extended to multi-channel settings, enabling downstream applications such as tool-agnostic safe handovers and context-aware pick-and-place.

## 6 Limitations

Although Point2Act is designed with efficiency in mind, it is not yet suitable for real-time, closed-loop control due to the overall processing time. The acquisition of multi-view images is essential for robustness against occlusion and noise, and thus cannot be omitted. However, the subsequent 3D reconstruction process remains a major bottleneck, requiring approximately 7 seconds. To mitigate this, future work could incorporate depth sensors for on-the-fly 3D reconstruction [46, 47, 48, 49]. Alternatively, real-time point tracking methods [50, 51] or keypoint-constrained control frameworks [26] could be employed to continuously update object states without the need for full 3D reconstruction at each timestep.

The auto-regressive nature of LLMs can slow down processing, particularly when generating lengthy outputs. While our point-based output significantly reduces processing time compared to verbose textual descriptions, delays can still occur when numerous points are relevant in the scene, such as in response to prompts like “point to all people in the concert.”

Moreover, our method focuses on identifying the most relevant 3D point in the scene rather than generating full segmentation masks. While this granularity is often sufficient for tasks like grasping, certain applications may benefit from region-level outputs. In such cases, our approach could be extended using techniques such as Set of Mark [52], where the MLLM response is treated as an index to retrieve an approximate mask. However, obtaining accurate masks remains inherently challenging: even with advances such as SAM [53], acquiring ground-truth masks is non-trivial, and the desired granularity level can vary depending on the task. Additionally, since each mark must be rendered into the scene, the marks themselves may occlude small or thin objects, making precise referencing more difficult, particularly in cluttered environments.

Finally, Point2Act currently relies on a server-grade GPU to run the MLLM. Although this setup enables strong performance, it results in considerable energy consumption, raising concerns about sustainability. Future work could explore model quantization or the development of more efficient LLM architectures to address these concerns.

## References

- [1] A. Radford, J. W. Kim, C. Hallacy, A. Ramesh, G. Goh, S. Agarwal, G. Sastry, A. Askell, P. Mishkin, J. Clark, et al. Learning transferable visual models from natural language supervision. In *International conference on machine learning*, pages 8748–8763. PmLR, 2021.
- [2] S. Kobayashi, E. Matsumoto, and V. Sitzmann. Decomposing nerf for editing via feature field distillation. *Advances in neural information processing systems*, 35:23311–23330, 2022.
- [3] J. Kerr, C. M. Kim, K. Goldberg, A. Kanazawa, and M. Tancik. Lurf: Language embedded radiance fields. In *Proceedings of the IEEE/CVF International Conference on Computer Vision*, pages 19729–19739, 2023.
- [4] M. Qin, W. Li, J. Zhou, H. Wang, and H. Pfister. Langsplat: 3d language gaussian splatting. In *Proceedings of the IEEE/CVF Conference on Computer Vision and Pattern Recognition*, pages 20051–20060, 2024.
- [5] W. Shen, G. Yang, A. Yu, J. Wong, L. P. Kaelbling, and P. Isola. Distilled feature fields enable few-shot language-guided manipulation. In *CoRL*, 2023.
- [6] A. Rashid, S. Sharma, C. M. Kim, J. Kerr, L. Y. Chen, A. Kanazawa, and K. Goldberg. Language embedded radiance fields for zero-shot task-oriented grasping. In *7th Annual Conference on Robot Learning*, 2023.
- [7] K. M. Jatavallabhula, A. Kuwajerwala, Q. Gu, M. Omama, T. Chen, A. Maalouf, S. Li, G. Iyer, S. Saryazdi, N. Keetha, et al. Conceptfusion: Open-set multimodal 3d mapping. *arXiv preprint arXiv:2302.07241*, 2023.

- [8] S. Koch, J. Wald, M. Colosi, N. Vaskevicius, P. Hermosilla, F. Tombari, and T. Ropinski. Relationfield: Relate anything in radiance fields. In *IEEE/CVF Conference on Computer Vision and Pattern Recognition (CVPR)*, 2025.
- [9] B. Mildenhall, P. P. Srinivasan, M. Tancik, J. T. Barron, R. Ramamoorthi, and R. Ng. Nerf: Representing scenes as neural radiance fields for view synthesis. *Communications of the ACM*, 65(1):99–106, 2021.
- [10] B. Kerbl, G. Kopanas, T. Leimkühler, and G. Drettakis. 3d gaussian splatting for real-time radiance field rendering. *ACM Transactions on Graphics*, 42(4), July 2023. URL <https://repo-sam.inria.fr/fungraph/3d-gaussian-splatting/>.
- [11] Y. Bhalgat, I. Laina, J. F. Henriques, A. Zisserman, and A. Vedaldi. N2f2: Hierarchical scene understanding with nested neural feature fields. In *European Conference on Computer Vision*, pages 197–214. Springer, 2024.
- [12] S. Zhi, T. Laidlow, S. Leutenegger, and A. J. Davison. In-place scene labelling and understanding with implicit scene representation. In *Proceedings of the IEEE/CVF International Conference on Computer Vision*, pages 15838–15847, 2021.
- [13] V. Tschernezki, I. Laina, D. Larlus, and A. Vedaldi. Neural feature fusion fields: 3d distillation of self-supervised 2d image representations. In *2022 International Conference on 3D Vision (3DV)*, pages 443–453. IEEE, 2022.
- [14] J. Ye, N. Wang, and X. Wang. Featurenerf: Learning generalizable nerfs by distilling foundation models. In *Proceedings of the IEEE/CVF International Conference on Computer Vision*, pages 8962–8973, 2023.
- [15] N. M. M. Shafiullah, C. Paxton, L. Pinto, S. Chintala, and A. Szlam. Clip-fields: Weakly supervised semantic fields for robotic memory. *arXiv preprint arXiv:2210.05663*, 2022.
- [16] P. Marza, L. Matignon, O. Simonin, and C. Wolf. Multi-object navigation with dynamically learned neural implicit representations. In *Proceedings of the IEEE/CVF International Conference on Computer Vision*, pages 11004–11015, 2023.
- [17] O. Kwon, J. Park, and S. Oh. Renderable neural radiance map for visual navigation. In *Proceedings of the IEEE/CVF Conference on Computer Vision and Pattern Recognition*, pages 9099–9108, 2023.
- [18] Q. Wang, H. Zhang, C. Deng, Y. You, H. Dong, Y. Zhu, and L. Guibas. Sparsedff: Sparse-view feature distillation for one-shot dexterous manipulation. *arXiv preprint arXiv:2310.16838*, 2023.
- [19] J. Lee, S. M. Kim, Y. Lee, and Y. M. Kim. Nfl: Normal field learning for 6-dof grasping of transparent objects. *IEEE Robotics and Automation Letters*, 9(1):819–826, 2023.
- [20] Q. Wang, C. Deng, T. G. W. Lum, Y. Chen, Y. Yang, J. Bohg, Y. Zhu, and L. Guibas. Neural attention field: Emerging point relevance in 3d scenes for one-shot dexterous grasping. *arXiv preprint arXiv:2410.23039*, 2024.
- [21] Y. Zheng, X. Chen, Y. Zheng, S. Gu, R. Yang, B. Jin, P. Li, C. Zhong, Z. Wang, L. Liu, et al. Gaussiangrasper: 3d language gaussian splatting for open-vocabulary robotic grasping. *IEEE Robotics and Automation Letters*, 2024.
- [22] Y. Wang, M. Zhang, Z. Li, T. Kelestemur, K. Driggs-Campbell, J. Wu, L. Fei-Fei, and Y. Li. D<sup>3</sup>fields: Dynamic 3d descriptor fields for zero-shot generalizable rearrangement. In *8th Annual Conference on Robot Learning*, 2024.

- [23] J. Liang, W. Huang, F. Xia, P. Xu, K. Hausman, B. Ichter, P. Florence, and A. Zeng. Code as policies: Language model programs for embodied control. In *2023 IEEE International Conference on Robotics and Automation (ICRA)*, pages 9493–9500. IEEE, 2023.
- [24] I. Singh, V. Blukis, A. Mousavian, A. Goyal, D. Xu, J. Tremblay, D. Fox, J. Thomason, and A. Garg. Progprompt: Generating situated robot task plans using large language models. In *2023 IEEE International Conference on Robotics and Automation (ICRA)*, pages 11523–11530. IEEE, 2023.
- [25] W. Huang, C. Wang, R. Zhang, Y. Li, J. Wu, and L. Fei-Fei. Voxposer: Composable 3d value maps for robotic manipulation with language models. *arXiv preprint arXiv:2307.05973*, 2023.
- [26] W. Huang, C. Wang, Y. Li, R. Zhang, and L. Fei-Fei. Rekep: Spatio-temporal reasoning of relational keypoint constraints for robotic manipulation. *arXiv preprint arXiv:2409.01652*, 2024.
- [27] A. Brohan, N. Brown, J. Carbajal, Y. Chebotar, X. Chen, K. Choromanski, T. Ding, D. Driess, A. Dubey, C. Finn, et al. Rt-2: Vision-language-action models transfer web knowledge to robotic control. *arXiv preprint arXiv:2307.15818*, 2023.
- [28] D. Driess, F. Xia, M. S. M. Sajjadi, C. Lynch, A. Chowdhery, B. Ichter, A. Wahid, J. Tompson, Q. Vuong, T. Yu, W. Huang, Y. Chebotar, P. Sermanet, D. Duckworth, S. Levine, V. Vanhoucke, K. Hausman, M. Toussaint, K. Greff, A. Zeng, I. Mordatch, and P. Florence. Palm-e: An embodied multimodal language model. *arXiv preprint arXiv:2303.03378*, 2023. URL <https://doi.org/10.48550/arXiv.2303.03378>.
- [29] A. O’Neill, A. Rehman, A. Maddukuri, A. Gupta, A. Padalkar, A. Lee, A. Pooley, A. Gupta, A. Mandlekar, A. Jain, et al. Open x-embodiment: Robotic learning datasets and rt-x models: Open x-embodiment collaboration 0. In *2024 IEEE International Conference on Robotics and Automation (ICRA)*, pages 6892–6903. IEEE, 2024.
- [30] O. M. Team, D. Ghosh, H. Walke, K. Pertsch, K. Black, O. Mees, S. Dasari, J. Hejna, T. Kreiman, C. Xu, et al. Octo: An open-source generalist robot policy. *arXiv preprint arXiv:2405.12213*, 2024.
- [31] K. Black, N. Brown, D. Driess, A. Esmail, M. Equi, C. Finn, N. Fusai, L. Groom, K. Hausman, B. Ichter, et al.  $\pi 0$ : A vision-language-action flow model for general robot control, 2024. URL <https://arxiv.org/abs/2410.24164>.
- [32] K. Fang, Y. Zhu, A. Garg, A. Kurenkov, V. Mehta, L. Fei-Fei, and S. Savarese. Learning task-oriented grasping for tool manipulation from simulated self-supervision. *The International Journal of Robotics Research*, 39(2-3):202–216, 2020.
- [33] C. Tang, D. Huang, W. Ge, W. Liu, and H. Zhang. Grasppt: Leveraging semantic knowledge from a large language model for task-oriented grasping. *IEEE Robotics and Automation Letters*, 8(11):7551–7558, 2023.
- [34] S. Li, S. Bhagat, J. Campbell, Y. Xie, W. Kim, K. Sycara, and S. Stepputtis. Shapegrasp: Zero-shot task-oriented grasping with large language models through geometric decomposition. In *2024 IEEE/RSJ International Conference on Intelligent Robots and Systems (IROS)*, pages 10527–10534. IEEE, 2024.
- [35] C. Tang, D. Huang, W. Dong, R. Xu, and H. Zhang. Foundationgrasp: Generalizable task-oriented grasping with foundation models. *IEEE Transactions on Automation Science and Engineering*, 2025.
- [36] W. Liu, A. Daruna, and S. Chernova. Cage: Context-aware grasping engine. In *2020 IEEE International Conference on Robotics and Automation (ICRA)*, pages 2550–2556. IEEE, 2020.

- [37] D.-C. Hoang, J. A. Stork, and T. Stoyanov. Context-aware grasp generation in cluttered scenes. In *2022 International Conference on Robotics and Automation (ICRA)*, pages 1492–1498. IEEE, 2022.
- [38] S. Jin, J. Xu, Y. Lei, and L. Zhang. Reasoning grasping via multimodal large language model. *arXiv preprint arXiv:2402.06798*, 2024.
- [39] M. Deitke, C. Clark, S. Lee, R. Tripathi, Y. Yang, J. S. Park, M. Salehi, N. Muennighoff, K. Lo, L. Soldaini, et al. Molmo and pixmo: Open weights and open data for state-of-the-art multimodal models. *arXiv preprint arXiv:2409.17146*, 2024.
- [40] H.-S. Fang, C. Wang, H. Fang, M. Gou, J. Liu, H. Yan, W. Liu, Y. Xie, and C. Lu. Anygrasp: Robust and efficient grasp perception in spatial and temporal domains. *IEEE Transactions on Robotics*, 39(5):3929–3945, 2023.
- [41] H. Law and J. Deng. Cornernet: Detecting objects as paired keypoints. In *Proceedings of the European conference on computer vision (ECCV)*, pages 734–750, 2018.
- [42] X. Dong, J. Bao, Y. Zheng, T. Zhang, D. Chen, H. Yang, M. Zeng, W. Zhang, L. Yuan, D. Chen, et al. Maskclip: Masked self-distillation advances contrastive language-image pretraining. In *Proceedings of the IEEE/CVF Conference on Computer Vision and Pattern Recognition*, pages 10995–11005, 2023.
- [43] J. H. Kang, P. Limcaoco, N. Dhanaraj, and S. K. Gupta. Safe robot to human tool handover to support effective collaboration. In *International Design Engineering Technical Conferences and Computers and Information in Engineering Conference*, volume 87363, page V008T08A088. American Society of Mechanical Engineers, 2023.
- [44] Z. Wang, Z. Liu, N. Ouporov, and S. Song. Contacthandover: Contact-guided robot-to-human object handover. In *2024 IEEE/RSJ International Conference on Intelligent Robots and Systems (IROS)*, pages 9916–9923. IEEE, 2024.
- [45] C. L. Blengini, P. D. C. Cheng, and M. Indri. Safe robot affordance-based grasping and handover for human-robot assistive applications. In *IECON 2024-50th Annual Conference of the IEEE Industrial Electronics Society*, pages 1–6. IEEE, 2024.
- [46] B. Curless and M. Levoy. A volumetric method for building complex models from range images. In *Proceedings of the 23rd annual conference on Computer graphics and interactive techniques*, pages 303–312, 1996.
- [47] R. A. Newcombe, S. Izadi, O. Hilliges, D. Molyneaux, D. Kim, A. J. Davison, P. Kohi, J. Shotton, S. Hodges, and A. Fitzgibbon. Kinectfusion: Real-time dense surface mapping and tracking. In *2011 10th IEEE international symposium on mixed and augmented reality*, pages 127–136. Ieee, 2011.
- [48] J. Shotton, B. Glocker, C. Zach, S. Izadi, A. Criminisi, and A. Fitzgibbon. Scene coordinate regression forests for camera relocalization in rgb-d images. In *Proceedings of the IEEE conference on computer vision and pattern recognition*, pages 2930–2937, 2013.
- [49] A. Zeng, S. Song, M. Nießner, M. Fisher, J. Xiao, and T. Funkhouser. 3dmatch: Learning local geometric descriptors from rgb-d reconstructions. In *CVPR*, 2017.
- [50] C. Doersch, Y. Yang, M. Vecerik, D. Gokay, A. Gupta, Y. Aytar, J. Carreira, and A. Zisserman. Tapir: Tracking any point with per-frame initialization and temporal refinement. In *Proceedings of the IEEE/CVF International Conference on Computer Vision*, pages 10061–10072, 2023.
- [51] M. Vecerik, C. Doersch, Y. Yang, T. Davchev, Y. Aytar, G. Zhou, R. Hadsell, L. Agapito, and J. Scholz. Robotap: Tracking arbitrary points for few-shot visual imitation. In *2024 IEEE International Conference on Robotics and Automation (ICRA)*, pages 5397–5403. IEEE, 2024.

- [52] J. Yang, H. Zhang, F. Li, X. Zou, C. Li, and J. Gao. Set-of-mark prompting unleashes extraordinary visual grounding in gpt-4v. *arXiv preprint arXiv:2310.11441*, 2023.
- [53] A. Kirillov, E. Mintun, N. Ravi, H. Mao, C. Rolland, L. Gustafson, T. Xiao, S. Whitehead, A. C. Berg, W.-Y. Lo, et al. Segment anything. In *Proceedings of the IEEE/CVF international conference on computer vision*, pages 4015–4026, 2023.
- [54] M. Quigley, K. Conley, B. Gerkey, J. Faust, T. Foote, J. Leibs, R. Wheeler, A. Y. Ng, et al. Ros: an open-source robot operating system. In *ICRA workshop on open source software*, volume 3, page 5. Kobe, 2009.
- [55] J. Luo, Z. Hu, C. Xu, Y. L. Tan, J. Berg, A. Sharma, S. Schaal, C. Finn, A. Gupta, and S. Levine. Serl: A software suite for sample-efficient robotic reinforcement learning. In *2024 IEEE International Conference on Robotics and Automation (ICRA)*, pages 16961–16969. IEEE, 2024.
- [56] H. Edelsbrunner, D. Kirkpatrick, and R. Seidel. On the shape of a set of points in the plane. *IEEE Transactions on information theory*, 29(4):551–559, 1983.
- [57] Q.-Y. Zhou, J. Park, and V. Koltun. Open3d: A modern library for 3d data processing. *arXiv preprint arXiv:1801.09847*, 2018.
- [58] S. F. Bhat, R. Birkl, D. Wofk, P. Wonka, and M. Müller. Zoedepth: Zero-shot transfer by combining relative and metric depth. *arXiv preprint arXiv:2302.12288*, 2023.

# Appendix

## A.1 Experimental Setup

### A.1.1 Hardware Setup

All experiments are conducted using a single NVIDIA RTX 4090 GPU for 3D reconstruction and grasp generation, and an NVIDIA RTX 6000 Ada for MLLM [39] querying. We use a Franka Emika Panda arm, with an Intel RealSense camera wrist-mounted via a 3D-printed mount to capture RGB images; its depth output is used only in the MLLM with Depth baseline. An additional laptop running a real-time kernel controls the robot, with communication handled via ROS [54]. Robot control is based on impedance control using the controller from SERL [55], which clips translational and rotational errors between the end-effector and the target pose to reduce abrupt accelerations.

### A.1.2 Context-Aware 3D Localization

**Occlusion-free Mask for Evaluation.** A critical component of our evaluation is obtaining occlusion-free ground truth masks, which are difficult to acquire in real-world scenarios. To address this, we first generate per-view 2D masks using the Segment Anything Model (SAM) [53]. These masks are then used to augment RGB images by attaching binary mask values as an additional channel. We train a NeRF model on this augmented data.

After training, we extract a 3D point cloud corresponding to the masked regions by selecting points with high mask activation ( $> 0.5$ ). We reconstruct a surface mesh from these points using the AlphaShape [56] algorithm implemented in open3d [57]. Finally, we render this mesh from each camera viewpoint to obtain consistent and occlusion-free pseudo ground truth masks. This pipeline allows us to evaluate 3D localization performance under challenging occlusions in a principled and reproducible manner.

**Relevancy scoring for baselines.** We provide a detailed explanation of the relevancy computation used in the baseline approaches, LERF [3] and F3RM [5]. Since raw CLIP [1] embedding similarity is not a reliable relevancy metric, LERF proposes a comparison-based scoring strategy. Given a set of canonical phrases such as “object”, “things”, “stuff”, and “texture”, the relevancy score  $r$  is defined as  $\min_i \frac{\exp(\phi_{\text{lang}} \cdot \phi_{\text{quer}})}{\exp(\phi_{\text{lang}} \cdot \phi_{\text{canon}}^i) + \exp(\phi_{\text{lang}} \cdot \phi_{\text{quer}})}$  where  $\phi_{\text{lang}}$  is the rendered language embedding,  $\phi_{\text{quer}}$  is the embedding of the target query, and  $\phi_{\text{canon}}^i$  is the embedding of the  $i$ -th canonical phrase. Intuitively, the score reflects how much closer the rendered language embedding is to the target query compared to generic canonical concepts. We adopt the same scoring strategy for F3RM.

**Complete List of Prompts.** To evaluate the 3D localization performance of Point2Act, we carefully design the prompt and the configuration of the scene. First, we define 5 prompt types as below:

- Object only: Direct references to an object instance by its name,
- Texture: Refers to objects based on surface appearance or material,
- Part: Targets a specific sub-region or component of an object,
- Spatial: Describes an object based on its spatial relation within the scene,
- Physical: Refers to physical properties inferred from context.

The complete list of prompts is in Table A1 and the example images are in Figure A9.

**Quantitative Results.** Table A2 provides the exact projection accuracy values for the details. We show the results for 300 iterations used for grasping, and 2000 iterations, which are sufficient for converging CLIP features.

Scene	Prompt Type	Query
Clutter 1	Object only	'Utility knife', 'Can'
	Texture	'The blue scissors', 'The green mug', 'The red mug', 'The yellow screwdriver'
	Part	'The handle of green mug', 'The cap of blue toothpaste' 'The tip of screwdriver', 'The blue handle of scissors'
	Spatial	'The paper cup lying on the table', 'The Scissors on the mug', 'The Scissors above utility knife'
	Physical	'The toothpaste closer to the soda can', 'The upright paper cup' 'The lightest cup'
Clutter 2	Object only	'The tape'
	Texture	'The yellow post-it', 'The blue post-it', 'The coke can'
	Part	'The green can', 'The black marker pen', 'The blue scissors' 'The handle of the blue scissors', 'The cap of the blue marker pen'
	Spatial	'The stapler on the tape', 'The post-it nearest to the tape' 'The utility knife below the black marker pen', 'The can lying upright on the table'
	Object only	'The screwdriver', 'The can', 'The pot'
Clutter 3	Texture	'The yellow screwdriver', 'The yellow paper cup', 'The aluminium can'
	Part	'The handle of yellow screwdriver', 'The tab of soda can'
	Spatial	'The cup closest to the soda can', 'The scissors placed higher' 'The handle of the cup closest to the soda can'
	Physical	'The lightest cup', 'The tallest cup', 'The heaviest cup'
	Markers 1	Object only
Texture		'The blue marker', 'The red marker'
Part		'The cap of blue marker', 'The cap of red marker'
Spatial		'The marker on the paper', 'The cap of the marker on the paper' 'The cap of the black marker outside the paper'
Markers 2		Texture
	Part	'The handle of green mug', 'The handle of red mug'
	Spatial	'The marker upside down', 'The handle of mug which contains blue marker' 'The handle of mug which contains red marker'
	Red	Object only
Texture		'The red mug', 'The red pen', 'The red marker', 'The red plier', 'The red can', 'The red toothpaste'
Part		'The handle of red mug', 'The cap of red marker', 'The handle of red plier', 'The cap of red toothpaste'
Green		Object only
	Texture	'The green can', 'The green note', 'The green sunglasses'
	Part	'The handle of green mug'
Blue	Object only	'The doll', 'The marker', 'The post-it', 'The fabric deodorizer'
	Texture	'The blue marker'
	Spatial	'The handle of scissors on the bear', 'The toothpaste closer to the blue marker'

Table A1: Complete list of prompts for each scene



Figure A9: Example scenes from our 3D localization experiments.

	LERF [3]	F3RM [5]	Point2Act (Ours)
300 iters	37.2%	57.7%	88.7%
2000 iters	59.3%	67.7%	87.9%

Table A2: Projection accuracy of 3D localization.

Scene	Prompt Type	Query
Mugs and Can	Part	‘The handle of red mug’, ‘The handle of green mug’, ‘The stem of roses’, ‘The flower of roses’
	Context	‘The handle of mug at the center’, ‘The handle of mug closer to the soda can’, ‘The handle of mug containing roses’
Scissors and Markers	Part	‘The cap of blue marker’, ‘The cap of red marker’, ‘The handle of blue scissors’, ‘The tip of red scissors’
	Context	‘cap of marker, that red scissors are pointing at’, ‘The tip of larger scissors’
Kitchen	Part	‘The handle of the kettle’, ‘The handle of spatula’
	Context	‘The end of the kettle where water comes out’, ‘where to grasp to carry the pan’, ‘The part to open the pan’
Tissue	Part	‘The tissue in the box’
	Context	‘Something to wipe spilled coffee’

Table A3: Complete list of prompts for each scene



Figure A10: Example scenes from our grasping experiments.

### A.1.3 Context-Aware Zero-Shot Robotic Grasping

**Implementation Details.** To generate the (object; part) pairs required by LERF-TOGO, we follow the instructions described in [6] and utilize GPT-4o. For example, given the prompt “Q: How can I safely lift the roses?”, the model returns “Basic action: grasp; Sequence: 1. roses 2. stems”, from which we extract the object and part components for evaluation.

We run 2000 iterations for LERF-TOGO following the original paper, and 300 iterations for both our method and F3RM for a fair comparison. To ensure fairness, we do not use the depth prediction network ZoeDepth [58]. While F3RM is originally a few-shot grasping method that requires a final grasp pose for optimization, we adapt it to a zero-shot setting by replacing the point-based relevancy field in our method with CLIP embeddings and keeping the rest of our pipeline unchanged. For the MLLM with depth baseline, we first capture a top-down view for the MLLM query, extract the relevant point, and apply a Gaussian blur kernel to generate a soft relevancy mask. Using the captured RGB-D and the resulting mask, we follow the same grasp selection procedure as in our method.

**Complete List of Prompts.** The complete list of prompts is in Table A3 and the example scenes are in Figure A10.

### A.1.4 Downstream Tasks

**Tool-agnostic Safe Handover.** To enable safe handover regardless of the object type or shape, we separately identify the graspable region and the hazardous (i.e., sharp or functional) region of the object using our 3D relevancy field. We then compute a *dangerous vector*, defined as the vector originating from the graspable point and pointing toward the hazardous region. This vector captures the relative spatial relationship between the two regions. To ensure safe interaction with a human, we align this dangerous vector with a pre-defined human-facing direction using a rigid transformation. As a result, the grasped object is oriented such that the dangerous part faces away from the human, allowing a tool-agnostic and context-aware handover.

**Context-aware Pick and Place.** We demonstrate a context-aware pick-and-place task where the robot must identify an object located outside a box and place it safely into the box. Using our

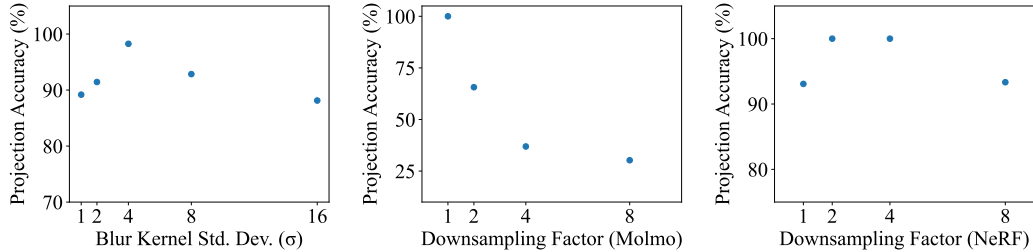


Figure A11: Projection accuracy across different ablation settings. Left: Effect of Gaussian blur kernel size on soft relevancy mask generation. Middle: Effect of image resolution on Molmo-based MLLM query performance. Right: Effect of image resolution on NeRF reconstruction.

language-conditioned 3D relevancy field, we localize the graspable part of the object (e.g., a handle) and a safe placement region within the box. To simulate a realistic and constrained placement scenario, we place a bubble wrap inside the box, which is used as the designated placement target. This soft region is detected through a visual-language query using the MLLM, such as “the best region to drop a fragile mug.” The robot first grasps the object at the identified graspable region, lifts it vertically by 20cm to avoid collisions, and then places it on the soft region inside the box.

## A.2 Ablation Study

### A.2.1 Effect of Gaussian Blur Strength

We evaluate the impact of varying Gaussian blur kernel sizes on the generation of the soft relevancy mask. Since the extracted 2D points tend to be sparse and noisy, applying a moderate blur helps produce a more stable mask by reducing isolated noise and reinforcing regions where multiple points overlap. As shown in the left plot of Figure A11, projection accuracy improves up to  $\sigma = 4$ , after which larger kernels begin to degrade performance due to excessive smoothing. Based on this observation, we fix the standard deviation to  $\sigma = 4$  for all experiments.

### A.2.2 Effect of Image Resolution

We analyze how image resolution affects two key components of our system: the Molmo-based MLLM query and NeRF reconstruction. Starting from a base resolution of  $640 \times 360$ , we systematically vary the downsampling factor and examine its influence on each stage.

For the MLLM query, reducing image resolution degrades the model’s ability to capture fine-grained contextual and spatial cues, which are crucial for precise language grounding. To evaluate this effect, we conduct an ablation study using multiple input resolutions. As shown in the middle plot of Figure A11, performance drops significantly below the  $640 \times 360$  threshold. We therefore adopt this resolution as the default setting for all MLLM queries in our experiments.

In contrast, NeRF training benefits from lower-resolution inputs, particularly under limited training iterations (e.g., 300). A key challenge in this low-iteration regime is the emergence of floater artifacts, which arise when rays fail to intersect consistently, leading to ambiguous supervision. While such issues are negligible in standard NeRF training, they become critical in our fast reconstruction setting. Lower-resolution images increase ray redundancy and enhance consistency across views. As shown in the right plot of Figure A11, reconstruction quality generally improves with moderate downsampling. However, overly aggressive downsampling (e.g., to  $80 \times 45$  with an  $8 \times$  reduction) compromises geometric detail, resulting in degraded performance. In all our experiments, we adopt a downsampling factor of 4, corresponding to an image resolution of  $160 \times 90$ .